Tellus (1993), 45A, 247–269
Printed in Belgium – all rights reserved

TELLUS
ISSN 0280–6495

Physical initialization using SSM/I rain rates

By T. N. KRISHNAMURTI*, H. S. BEDI and KEVIN INGLES, *Department of Meteorology, Florida State University, Tallahassee, FL 32306-3034, USA*

(Manuscript received 17 August 1992; in final form 17 May 1993)

ABSTRACT

Following our recent study on physical initialization for tropical prediction using rain rates based on outgoing long-wave radiation, the present study demonstrates a major improvement from the use of microwave radiance based rain rates. A rain rate algorithm is used on the data from a special sensor microwave instrument (SSM/I). The initialization, as before, uses a reverse surface similarity theory, a reverse cumulus parameterization algorithm and a bisection method to minimize the difference between satellite-based and the model-based outgoing long-wave radiation. These are invoked within a preforecast Newtonian relaxation phase of the initialization. These tests are carried out with a high-resolution global spectral model. The impact of the initialization on forecast is tested for a complex triple typhoon scenario over the Western Pacific Ocean during September 1987. A major impact from the inclusion of the SSM/I is demonstrated. Also addressed are the spin-up issues related to the typhoon structure and the improved water budget from the physical initialization.

1. Introduction

This paper is a continuation of our recent study (Krishnamurti et al., 1991) on the incorporation of "observed rain rates" in the initialization of a numerical weather prediction model. Lacking an adequate network of surface and upper air observations, the inclusion of the satellite based rain rates improves the overall analysis over the tropical belt via physical initialization.

The US Air Force Satellite under the Defense Meteorology Satellite Program (DMSP) carried an array of passive microwave radiometer sensors that were specifically designed to provide measures of rain rates. (A list of acronyms is presented in Table 1.) Another useful product for the measures of rain rates comes from the outgoing longwave radiation (OLR) sensed by infrared (IR) channels in NOAA/TIROS series of satellites.

The microwave radiometric data have not been found very useful over regions of high sloping terrain. The OLR measures tend to produce a broad pattern of rain, largely arising from cirrus canopies over tropical cloud clusters. The broad patterns do not usually agree with the much sharper rainfall signatures of the microwave radiometric measurements. Thus we have noted that the two methods have some serious defects. However, a combination of some of the useful aspects of these rain measures, i.e., from the OLR over the land and from the microwave radiometer over the oceans, could be used in a complementary manner to produce more useful rainfall measures for numerical weather prediction.

Earlier satellite systems with microwave radiometry were limited to the highest i.e., the 37 GHz frequency channel. DMSP-SSM/I provided an additional 85.5 GHz dual polarized channel, which is very sensitive to the volume scattering by precipitation and can provide precipitation field over the land and oceans with a proper combinations of other channels of lower frequencies. The SSM/I DMSP-F8 was launched in June 1987 in a near polar sun synchronous orbit with horizontal (HH) and vertical (VV) polarization channels of 85.5, 37.0 and 19.35 GHz and a single vertical polarization (VV) channel of 22.235 GHz. The

* Corresponding author.

Table 1. *Acronyms*

DMSP	Defense Meteorology Satellite Program
ECMWF	European Center for Medium Range Weather Forecasts
FSU	Florida State University
GEWEX	Global Energy and Water Cycle Experiment
GHz	Giga Hertz
HH	Horizontal
IR	Infrared
ITCZ	Intertropical Convergence Zone
JTWC	Joint Typhoon Warning Center
MONEX	Monsoon Experiment
NASA	National Atmospheric and Space Agency
NCAR	National Center for Atmospheric Research
NOAA	National Center for Atmospheric Administration
OI	Optimal Interpolation
OLR	Outgoing Longwave Radiation
Q2	Apparent moisture sink
SCRI	Supercomputer Computational Research Institute
SI	Spectral Interpolation
SSM/I	Special Sensor Microwave Instrument
TB	Brightness Temperatures
TIROS	Television Infrared Observation Satellite
TOGA	Tropical Ocean and Global Atmospheric Program
TOGA-COARE	TOGA-Coupled Ocean Atmosphere Response Experiment
TRMM	Tropical Rainfall Measuring Mission
UTC	Coordinated Universal Time
VV	Vertical

spatial resolution of these channels are (16×14), (38×30), (70×45) and (60×40) km, respectively.

The OLR rain rates are based on a histogram method proposed by Janowiak and Arkin (1991). Here one makes use of class intervals of rain rates and the corresponding spread of OLR values to develop a histogram method for the rain rates from a reliable database. The class-interval histograms provide a means to translate the OLR values to rain rates.

In the present study we have used rainfall estimates based on a mix of OLR and SSM/I algorithms. This procedure is described in Subsection 3.3.

The incorporation of rain rates within a physical initialization procedure follows Krishnamurti et al. (1991). It allows for a model spin-up consistent with the prescribed rain rates. In the process of spin-up the divergence, the moisture and the diabatic heating respond to the imposed precipitation during a preforecast assimilation (nudging) phase.

The main objective of this paper is to test the usefulness of the OLR and SSM/I mix rain rate algorithm within an initialization-prediction exercise via a global model. For this purpose we have used a three typhoon scenario over the Western Pacific Ocean during September 1987 as a case study. In this paper we have examined the rain rates, the extent to which they are accepted by the model during the physical initialization, and the impact of initialization of the rainfall forecasts, the surface fluxes, the water budgets and the overall forecast skills.

2. FSU global spectral model

The global model used in this study is identical in all respects (except for the rain rate input) to that used in Krishnamurti et al. (1991). The following is an outline of the global model:

(a) Independent variables: (x, y, σ, t).

(b) Dependent variables: vorticity, divergence, surface pressure, vertical velocity, temperature and humidity.

(c) Horizontal resolution: Triangular 106 waves.

(d) Vertical resolution: 14 layers between roughly 50 and 1000 mb.

(e) Semi-implicit time differencing scheme.

(f) Envelope orography (Wallace et al., 1983).

(g) Centered differences in the vertical for all variables except humidity which is handled by an upstream differencing scheme.

(h) Fourth order horizontal diffusion (Kanamitsu et al., 1983).

(i) Kuo-type cumulus parameterization (Kuo, 1965, 1974; Krishnamurti et al., 1983).

(j) Shallow convection (Tiedke, 1984).

(k) Dry convective adjustment.

(l) Large scale condensation (Kanamitsu, 1975).

(m) Surface fluxes via similarity theory (Businger et al., 1971).

(n) Vertical distribution of fluxes utilizing diffusive formulation where the exchange coefficients are functions of the Richardson number (Louis, 1979).

(o) Long and shortwave radiative fluxes based on a band model, (Harshvardan and Corsetti, 1984; Lacis and Hansen, 1974).

(p) Diurnal cycle.

(q) Parameterization of low, middle and high clouds based on threshold relative humidity for radiative transfer calculations.

(r) Surface energy balance coupled to the similarity theory (Krishnamurti et al., 1991).

(s) Nonlinear normal mode initialization -5 vertical modes (Kitade, 1983).

(t) Physical initialization.

3. The design of experiment

3.1. The control experiment

In the present study, we provide a comparison of results for the two sets of experiments, one a control experiment and the other one that invokes the SSM/I rain rates within the physical initialization. The control experiment does not use the satellite or the OLR based rain rates in its initialization. This experiment utilizes the ECMWF analysis for the data fields at day 0 of forecasts which is subjected to nonlinear normal mode initialization with physics to define its initial state.

3.2. The physical initialization

The physical initialization follows our recent work, Krishnamurti et al. (1991). This entails several steps:

(i) Preparation of rainfall totals based on OLR, SSM/I and raingauge data sets during a 24-h period prior to the start of the forecast.

(ii) Calculations of surface flux of moisture from the difference between the vertically integrated apparent moisture sink (Q2 following Yanai et al., 1973) and the rainfall rates.

(iii) Use of a reverse similarity theory to obtain the humidity variable at the top of the constant flux layer consistent with the moisture fluxes.

(iv) Vertical restructuring of the moisture variable consistent with the observed rain rates using a reverse cumulus parameterization algorithm.

(v) A further restructuring of the moisture variable in the upper troposphere using a bisection method that minimizes the difference between the "satellite based" and the "model based" outgoing longwave radiations.

(vi) A newtonian relaxation phase between hour -24 to hour 0 of forecast where the model is spun up to accept, as closely as possible, the observed rain rates and the modified humidity field. During this step the vorticity, divergence and surface pressure fields are nudged to their preassigned values at hour 0. For this the equation for dynamic relaxation takes the form

$$\frac{\partial A_l^m}{\partial t} = N(A_l^{\circ m} - A_l^m). \tag{1}$$

Its finite difference approximation may be written as:

$$\frac{A_l^m(t+\Delta t) - A_l^{*m}(t+\Delta t)}{2\,\Delta t} = N(A_l^{\circ m}(t+\Delta t) - A_l^m(t+\Delta t)) \tag{2}$$

or

$$A_l^m(t+\Delta t) = (A_l^{*m}(t+\Delta t) + 2N\,\Delta t\, A_l^m(t+\Delta t))/(1+2N\,\Delta t). \tag{3}$$

Here $A_l^{*m}(t+\Delta t)$ is a predicted value of A_l^m at time $(t+\Delta t)$ prior to Newtonian relaxation, and

$A_I^m(t+\Delta t)$ is its final value achieved after relaxation. It may be noted that the relaxed value is the weighted average of the model predicted value and the observed value, with weights depending upon nudging coefficient N. For the nudging of vorticity field we used a nudging coefficient of 1.0×10^{-4}, whereas divergence and surface pressure fields were nudged using a weaker coefficient of 0.5×10^{-4}. With this the diabatic heating and the divergence field are allowed to undergo a spin-up more freely than the rotational part of the motion field.

The theoretical framework for the physical initialization is presented in detail in Krishnamurti et al. (1991).

3.3. *Precipitation methodology*

In our study we use a mix of OLR and SSM/I based rain rate algorithms. Given the cirrus canopies over tropical cloud clusters (and even over mesoscale cloud lines) the OLR derived rain tends to yield an excessive lateral spread as the cold black body temperatures of the cirrus anvils are translated as rain areas. The SSM/I rain is generally much more localized and appears to describe the precipitating hydrometeors more realistically. The OLR based rain in our study is based on a calibration of satellite based OLR values and the MONEX raingauge network. Fig. 1 illustrates schematically the nature of this spread of OLR rain as compared the SSM/I rain.

The SSM/I rain rates are obtained from the algorithm following Olson et al. (1990). As described in Gairola and Krishnamurti (1992), we have used an exponential form of retrieval equation using 85.5 (HH, VV), 37.0 (VV), 19.35 (VV) and 22.235 (VV) GHz frequencies for retrieving of precipitation over land and oceans. The upwelling microwave radiation in all these channels were first retrieved in the form of brightness temperatures (TB). The algorithms for the retrieval of the rain rate R, as a function of collocated SSM/I TB's were based on regressing the TB's against rainfall rates in a step-wise multiple linear regression. The following algorithms recommended by Olson et al. (1990) based on such a regression procedure for precipitation retrieval in the tropics were used for land and oceans respectively:

(I) For rainfall over the land

$$R = \exp(3.29716 - 0.01290\ \text{TB85VV} + 0.0087\ \text{TB85HH}) - 8.0\ \text{mm/h} \quad (4)$$

(II) For rainfall over the oceans

$$R = \exp(3.06231 - 0.0056036\ \text{TB85VV} + 0.0029478\ \text{TB85HH} - 0.0018119\ \text{TB37VV} - 0.00750\ \text{TB22VV} + 0.0097550\ \text{TB19VV}) - 8.0\ \text{mm/h} \quad (5)$$

In case, when the 85 GHz channels were unusuable then

(I) For rainfall over the land:

$$R = \exp(-17.76849 - 0.09612\ \text{TB37VV} + 0.15678\ \text{TB19VV}) - 1.0\ \text{mm/h}, \quad (6)$$

(II) For the rainfall over the oceans:

$$R = \exp(5.10196 - 0.05378\ \text{TB37VV} + 0.02766\ \text{TB37HH} + 0.01373\ \text{TB19VV}) - 2.0\ \text{mm/h}, \quad (7)$$

were used.

As a part of the rain rate retrieval process, these relationships were determined using collocated SSM/I data and radar rainfall observations.

It was noted that the SSM/I describes the ITCZ rain quite well, i.e., the monthly mean rain at neighboring island stations and the SSM/I based oceanic rain show a close agreement, Gairola and Krishnamurti (1992). However, over land areas the SSM/I rain shows large departures from the raingauge measures.

Thus it was felt that we need to develop some form of sharpened OLR rain as a first guess field

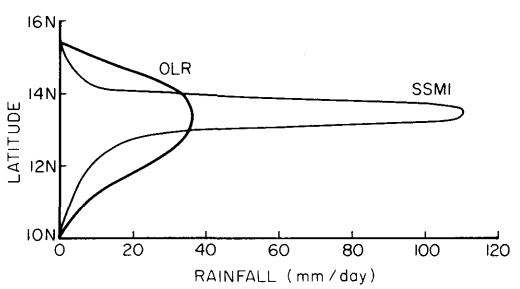

Fig. 1. Schematic spatial profile of an OLR based rain compared to that of an SSM/I based rain.

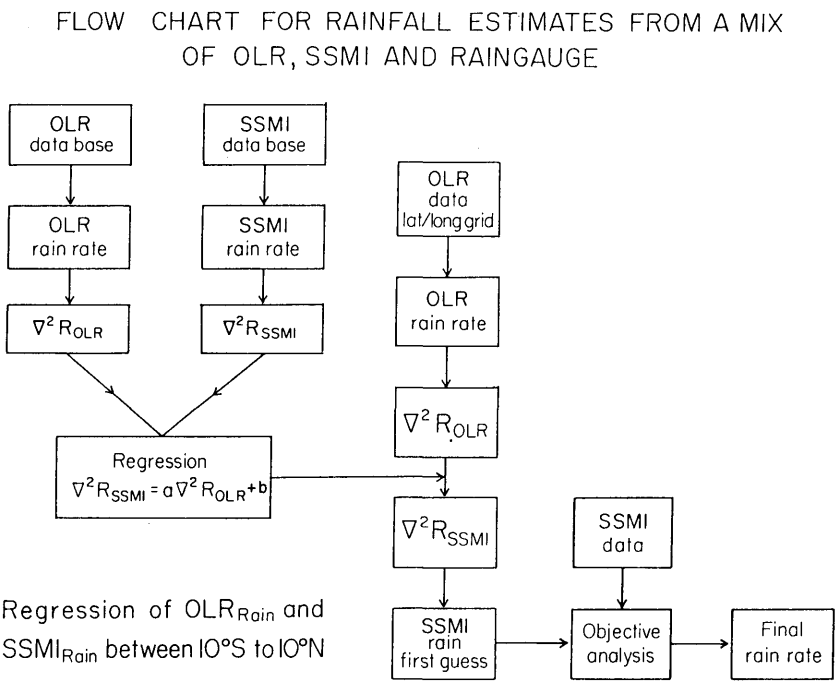

Fig. 2. Flow chart for the rainfall computation methodology. The left half of the flow chart provides a statistical algorithm for the sharpening of the OLR rain while the right half shows its application to a case study.

which overcomes the undesirable spread of the OLR rain. Fig. 2 illustrates a flow chart of our rainfall methodology, which is based on Gairola and Krishnamurti (1992). This contains two parts. The left half of this illustration describes a regression procedure based on 3 months of OLR and SSM/I data sets over the equatorial oceans, between $\pm 10°$, that provides a sharpening function for the OLR rain. This is done by regressing the ∇^2 of SSM/I rain against the ∇^2 of OLR rain. The linear regression coefficients are used to obtain a sharpened OLR rain as a first guess field from an objective analysis of the SSM/I rain for individual case histories. Details on the regression relation are given in Gairola and Krishnamurti (1991).

The spatial resolution of the SSM/I data at the 85.5, 37.0, 22.235 and 19.35 Gigahertz (GHz) data were respectively 16×14, 38×30, 60×40 and 70×45 km. Thus, on the average, we are able to resolve rain rates on roughly 50 km^2 along satellite swaths. This is a finer resolution than that of the OLR data which was available at roughly 250 km^2. The sharpening alluded to here was necessary to match the model resolution. The transform grid separation at the resolution T106 of the spectral model is around 100 km. The SSM/I rain rates matched the model rain rates more closely than those of OLR. This is partly attributed to the resolution of the rain rate data sets and partly to the deficiencies of the OLR spread alluded to earlier.

A sample sequence of global tropical 24 hourly rainfall totals are shown in Fig. 3 (a, b and c). This covers the period 6 to 8 September 1987. The rainfall over the oceans largely reflects the rainfall from SSM/I algorithm, while over the land areas it reflects the sharpened OLR rainfall as implied by Fig. 2. The global rainfall field shows the rainfall over the ITCZ, the typhoons, the monsoon and tropical depressions and the mid-latitude frontal extensions into the tropics. The fields are quite sharp over the oceans and the analysis is able to resolve rainfall rates in excess of 100 mm/day over several of these active tropical systems. We shall not provide a comparison of the SSM/I based and the OLR based rain rates here, that is covered in some detail by Gairola and Krishnamurti (1992).

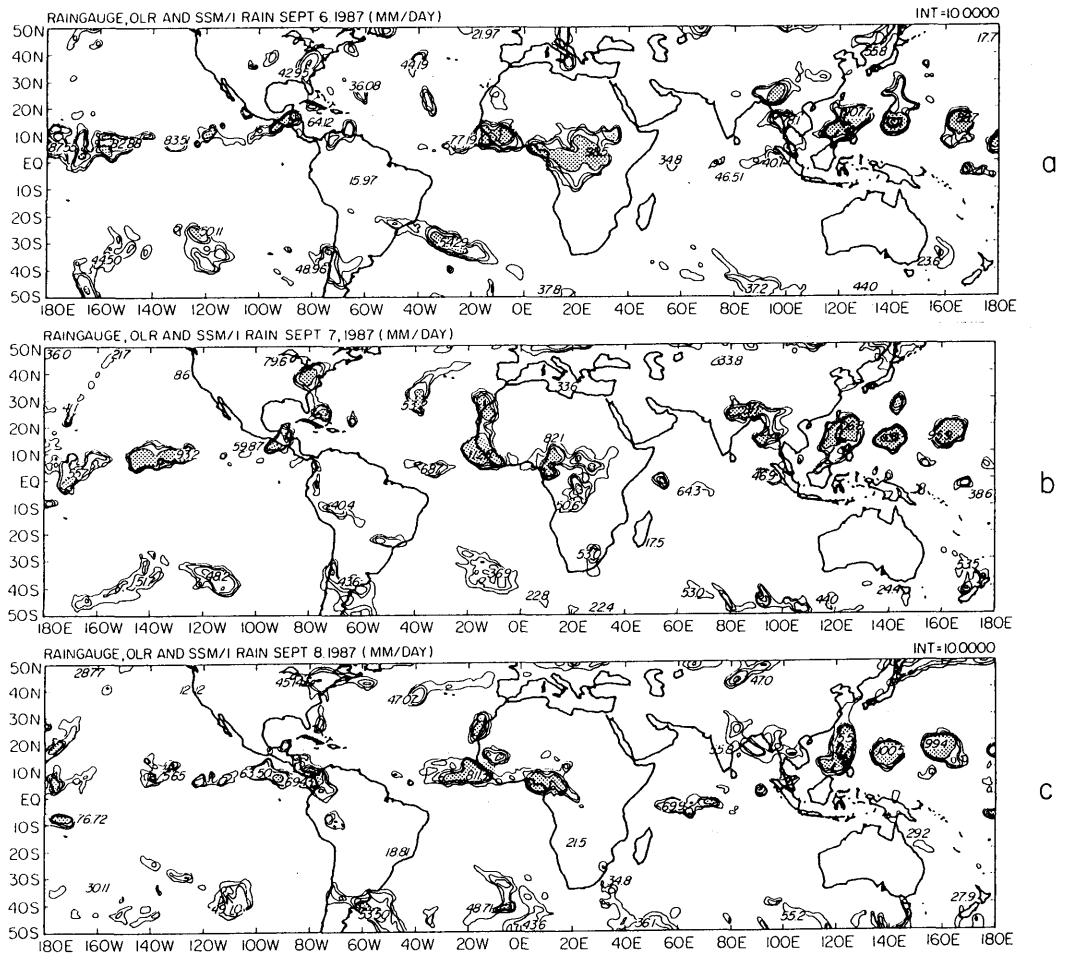

Fig. 3. Sample final 24 hourly rainfall from a mix of sharpened OLR and the SSM/I data sets. Unit: mm/day. Shaded areas indicate rainfall more than 40 mm/day. (a) 5 to 6 September 1987. (b) 6 to 7 September 1987. (c) 7 to 8 September 1987.

4. Case history

In this paper we have used a triple typhoon event to illustrate the impact of the SSM/I rain on the physical initialization. Fig. 4 is a satellite IR imagery taken on 9 September 1987 at around 00 UTC. This illustrates the three typhoons named (from west to east) Gerald, Freda, and Holly.

Gerald was the western most storm of this family. It formed just east of Luzon on 6 September and moved northwestwards and made a landfall over China on 10 September around 1200 UTC. That was a storm of moderate intensity; the maximum winds reached only around 52 ms^{-1} on 7 September. Freda formed on 7 September. After an initial northwesterly movement it recurved at around 137° E, and attained a maximum wind of around 62 ms^{-1} just after recurvature at around 17° N on 10 September. The eastern most typhoon, Holly, was a super typhoon whose recurvature occurred close to 156° E. This storm formed around 7 September and attained a maximum wind of around 70 ms^{-1} on 9 September. This storm, as well as Freda, remained over the

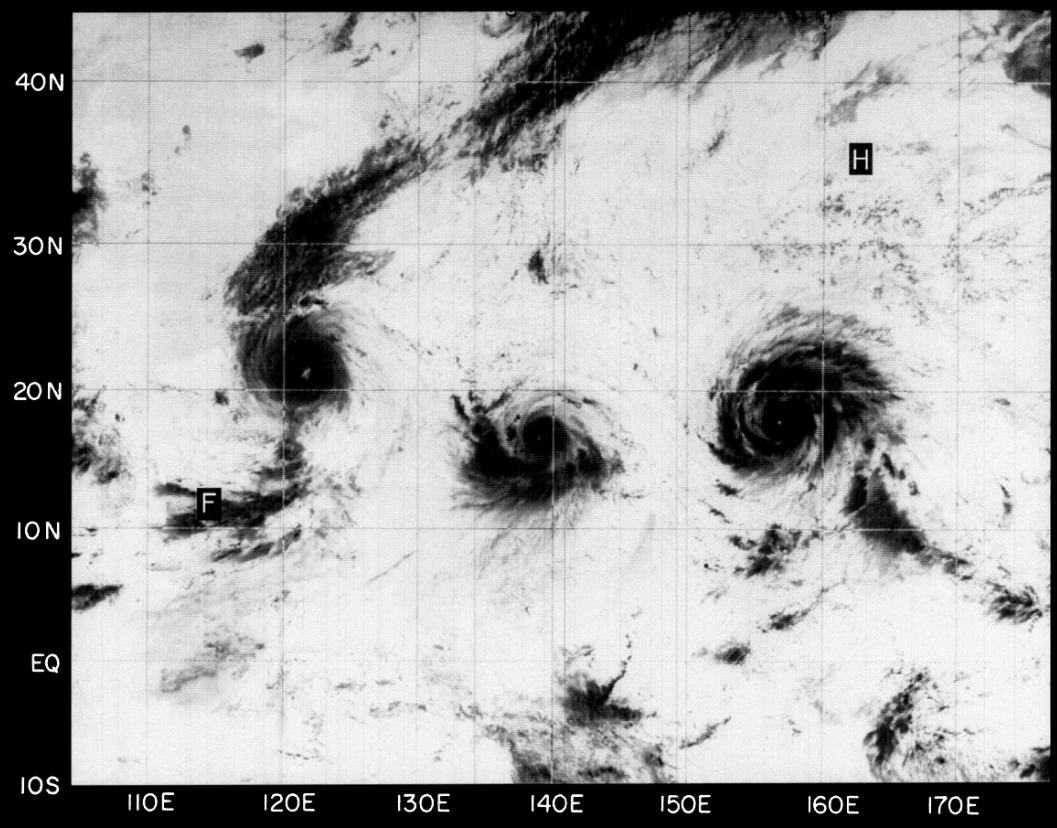

Fig. 4. Satellite IR imagery showing the three typhoons: From west to east, they are, Gerald, Freda and Holly, 9 September 1987.

ocean during its entire life history. The tracks of these storms based on the annual storm history prepared by Joint Typhoon Warning Center (JTWC), Guam (1987) will be presented in our discussion of their forecast. The surface maximum winds during their depression and storm stages ranged from 15 to 17 ms^{-1} (depression) and 52 to 70 ms^{-1} (typhoon stage). All of these storms formed along the Intertropical Convergence Zone (ITCZ) of the Western Pacific Ocean. This part of the ITCZ is also labelled as a monsoon trough by the JTWC, Guam. It is characterized by a family of vortical disturbances with easterlies to its north and westerlies to its south. Some of these vortices develop into typhoons over this part of the Pacific Ocean. The selection of the triple typhoon case was made in order to provide a severe test of the proposed physical initialization scheme. The triple typhoons have a tendency to interact with each other. The descending air around each storm, if not properly handled by a numerical prediction model, can easily affect the neighbor and result in an early demise of a storm. That was in fact noted in a control experiment. The size, intensity and structure of these storms, during the initialization, are somewhat critical for the predictions of the life cycle and storm tracks.

The initial state (i.e., $t=0$) for the prediction experiments was selected on 6 September 1987 at 1200 UTC. The physical initialization was carried out between hours-24 and 0 which commences on 5 September 1987 at 1200 UTC.

At the initial time the maximum winds at 850 mb (from the ECMWF analysis) were of the order of 18, 12 and 15 ms^{-1} for the storms Gerald, Freda and Holly respectively. These are

considerably lower than the estimated maximum winds provided by the JTWC at Guam which were of the order of 28, 26, and 32 ms^{-1} respectively. The westerly monsoon flow near 5°N extended to almost 150°E. Freda and Gerald were located on the cyclonic shear side of this monsoon current. At 200 mbs the most striking feature was the diffluent flow which was present over each of these typhoons at the initial time of the forecast experiments.

5. Results of experiments

5.1. Spin-up of surface fluxes during the physical initialization

The physical initialization results in a robust air-sea coupling. Here we illustrate the spin-up of the fluxes during the physical initialization. Fig. 5 (a, b, c, d, e) shows the spin-up of the latent heat flux between hours −24 and 0. The surface fluxes at hour −24 show somewhat of a disorganized pattern; the maximum value of the latent heat flux is of the order 300 watts/m^2. By hour −6, i.e., after 18 h of nudging the fluxes associated with the typhoons acquire a high degree of organization. This is evidently related to the spin-up of the storm's surface circulation. The spin-up of the surface wind field shows a more coherent organization of the typhoon structures. The spin-up accomplishes a more robust coupling of the ocean and the typhoons via these fluxes; this coupling appears to be important for the medium range forecasts.

The Newtonian relaxation does not appear to enhance the maximum value of the surface fluxes. It does, however, produce a quasisymmetric organization of the fluxes around the storm's center of circulation. The organization of fluxes appears to be important for the coupling of the storm with the ocean. This appears to maintain the storm for a longer time in the forecast experiment as compared to the control experiment. In the latter case the fluxes appear to be more disorganized with respect to the storm's center, and a proper coupling between the storm and the oceanic fluxes does not seem to occur during the forecast.

5.2. Spin-up of typhoon circulations during the physical initialization

The difference of the velocity potential and the stream function between hour −24 and hour 0 for the SSM/I run gives us a measure of the spin-up by physical initialization.

The prescribed rain augments the convective heating and spins up the divergent part of the wind. A weak nudging of the divergent part of the wind (nudging coefficient, 0.5×10^{-4}) during the physical initialization permits it to respond to the imposed rain rates. Although the rotational part is somewhat less weakly nudged (nudging coefficient, 1.0×10^{-4}), the aforementioned large change in the divergent wind accounts for a substantial spin-up of the rotational wind components as well and hence of the typhoon circulations. Fig. 6 shows this spin-up over the lower and the upper troposphere. The top panels a and b show the spin-up of the stream function (ψ) and the velocity potential (χ) at 200 mb respectively. The corresponding bottom panels c and d, respectively, show the spin-up of ψ and χ at 850 mb. These four panels show the changes which occurred in these fields during the physical initialization i.e., from hour −24 to hour 0 of nudging. They show that both ψ and χ exhibit a spin-up in this period throughout the troposphere. It is apparent from this diagram that the physical initialization builds the intensity of the cyclonic circulation (rotational flow) in the lower troposphere as well as that of the anticyclonic circulation in the upper troposphere. Thus it also effectively spins up the warm core of the three typhoons. The temperature field is permitted to freely float during the nudging process and the spin-up of the divergence and the consequent generation of the rotational circulation and its vertical gradient permits the evolution of a realistic warm core. One can assess the predictive capability of the warm core from the vertical cross sections of the equivalent potential temperature θ_e. Near the center of the typhoons θ_e acquires a near constant value along the vertical from the deep moist adiabatic ascent of air to the top of the troposphere. The large θ_e values along this vertical axis arise due to increase of moisture (saturation) and due to the formation of the warm core. The control experiment failed to show these features for all of the three typhoons. This is illustrated via the θ_e distributions in the three vertical cross sections on the top panels of Fig. 7. The bottom panels of this illustration, Fig. 7, shows the θ_e cross-sections for the SSM/I experiment where a clear eye wall like feature is present for all 3 typhoons. Relatively lesser increases in the θ_e value away from the storm

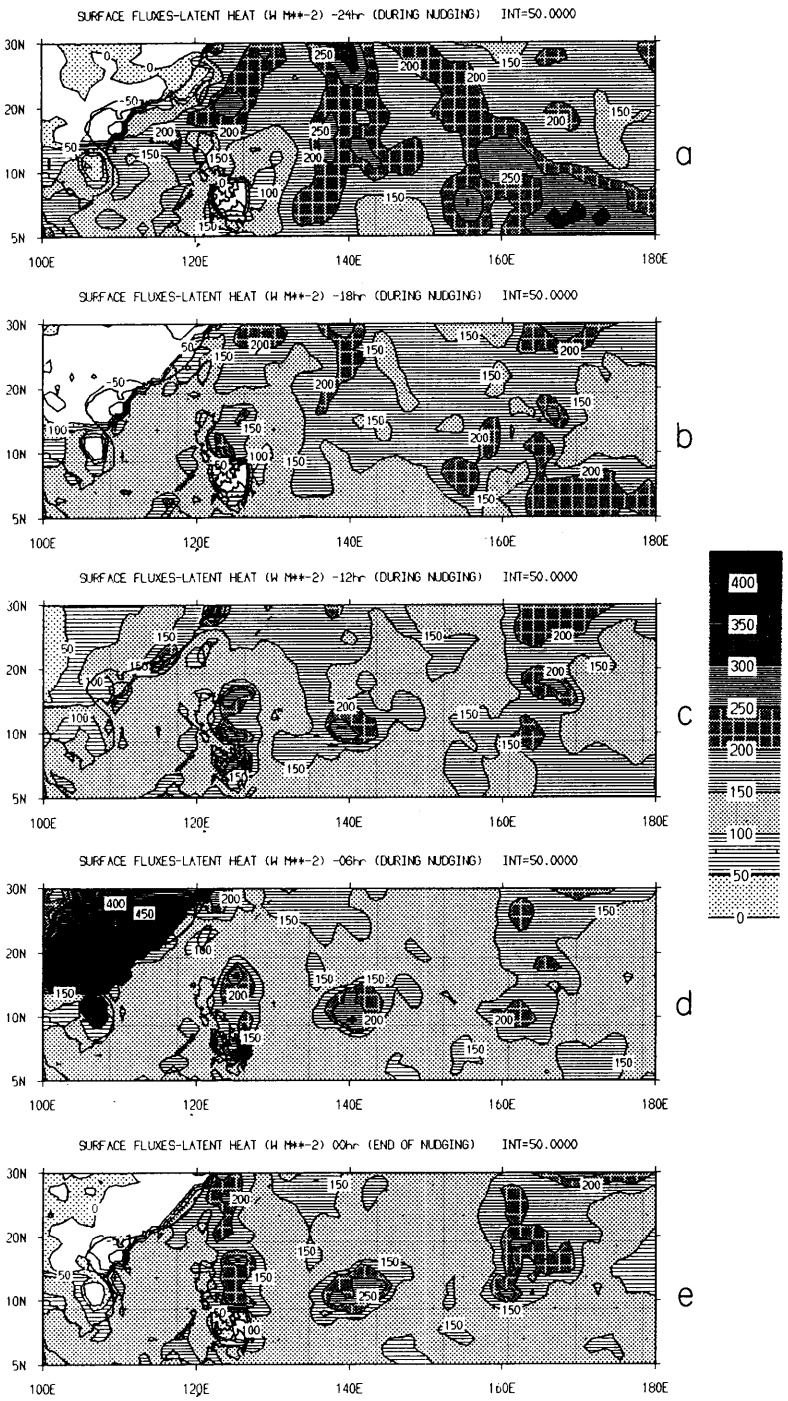

Fig. 5. The evolution of surface heat flux during the spin-up of the nudging phase. Units: W/m^2. The panels (a) through (e) cover the period hour −24 to hour 0 for every 6 h. The scale of shading is shown on the right.

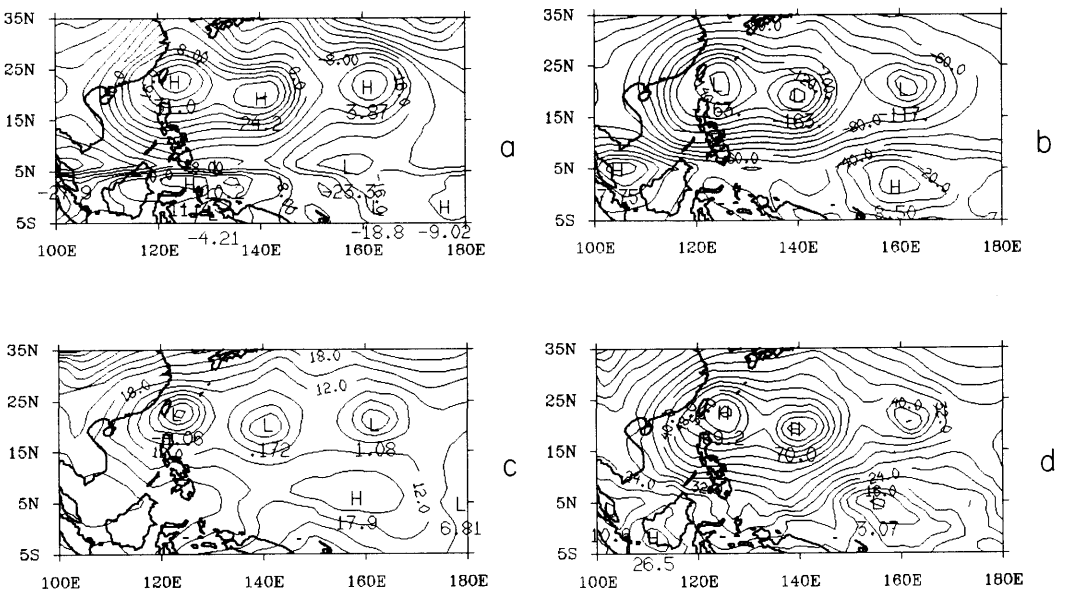

Fig. 6. Spin-up of the streamfunction ψ and the velocity potential χ at 200 mb top panels (a) and (b) respectively and at 850 mb bottom panels (c) and (d), respectively. The spin-up here denotes field values at hour zero minus its values at hour -24 of physical initialization phase. Units: $\times 10^5$ m^2 sec^{-1}.

cores appear to be due to subsidence of air in the storm environment. These are the results on day 3 of the forecast. The same results were seen on days 4 through 6 of forecast as well. This shows that an improved initialization contributes to an improvement in the predicted structure of the typhoons. The spin-up of the velocity potential clearly indicates the enhancement of the divergent inflow in the lower troposphere and of the divergent outflow in the upper troposphere over the three typhoons. This is one of the major impacts of the physical initialization. The control experiment during its first 24-h forecast did not exhibit any significant spin-up of the typhoon circulation. Typhoon Gerald was maintained reasonably well during the first 24 h in the control forecast but the other two storms showed a marked decline in their intensity.

5.3. *Spin-up of precipitation*

The precipitation spins up during the physical initialization. The model gradually incorporates the SSM/I rain as the polar orbitor swaths bring in more and more microwave radiance information. This data is incorporated in an asynoptic manner via the reverse similarity and the reverse cumulus parameterization algorithms and is relaxed for the next 6 h prior to the accumulation of new data from additional swaths. It should be noted that the OLR rain is used as a first guess (in our rain rate algorithms) and the SSM/I rain takes precedence over it where and when it becomes available over the oceanic areas. A summary of how the precipitation is handled by the physical initialization is presented in Table 2 (a and b). This table shows the results of rainfall spin-up during the preforecast period, i.e., between hours -24 and 0 over the global tropical and a Pacific Ocean domain enclosing the region of three typhoons. The first column shows the model based mean rainfall rates over the domains. The second column shows the observed rainfall rates which are largely based on SSM/I data sets. The ratios of the model based and the observed rain and their correlation coefficients are shown in columns 3 and 4. The model starts out during the initial three hours with a correlation coefficient of 0.57 for the global belt and of 0.65 for the Pacific typhoon belt; during the course of the physical initialization these respective correlation coefficients increase to 0.85 and 0.91.

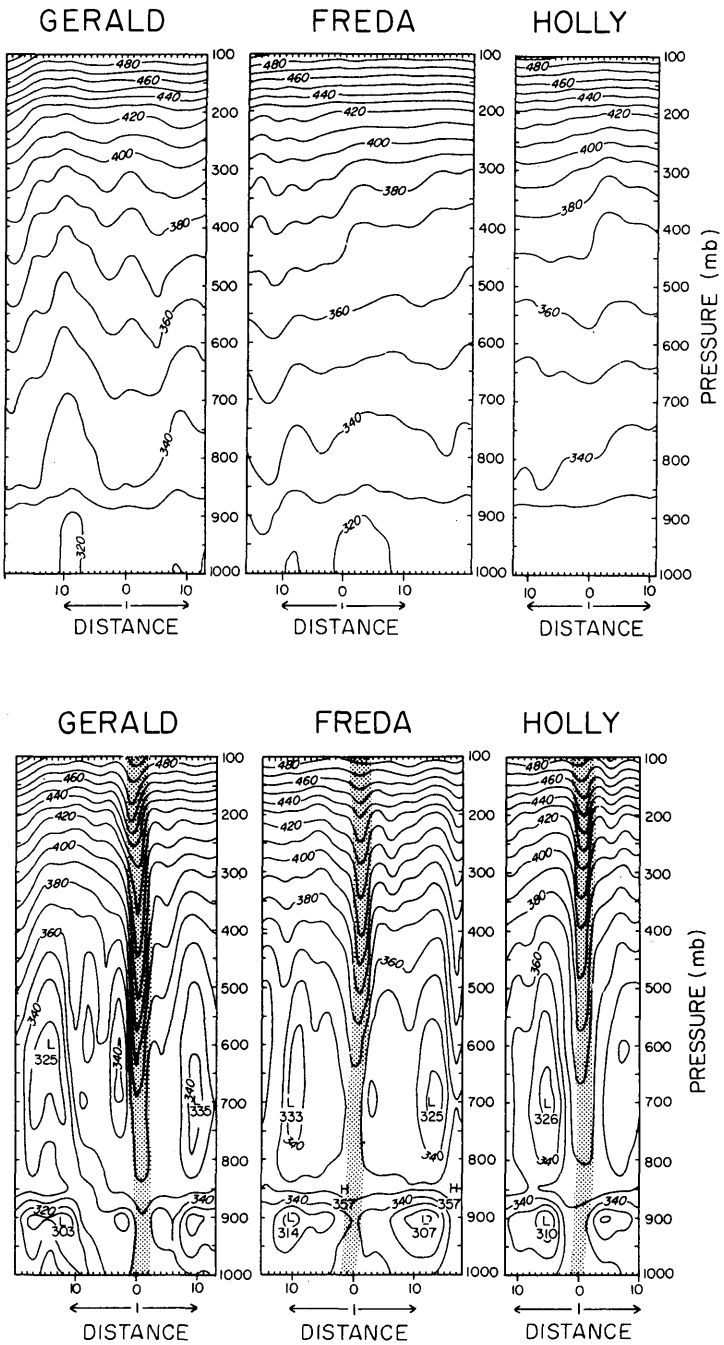

Fig. 7. Vertical cross section of the equivalent potential temperature θ_e (west to east) across the three typhoons. Abscissae show the distance from the storm center in terms of model grid interval (one grid interval = 0.94° long). Top panel shows the results for the control experiments for each of the three typhoons Gerald, Freda and Holly. Bottom panels illustrates the same for the SSM/I experiment. Units: degree K.

Table 2. *Spinup of rainfall during nudging*

(a) Global Tropical Belt (30°S to 30°N)

Hour	Model rain (mm/day)	SSMI rain (mm/day)	Ratio (model/SSMI)	Correlation coefficient
−21	2.30	4.28	0.54	0.57
−18	3.06	4.26	0.72	0.71
−15	3.35	4.23	0.79	0.79
−12	3.40	4.21	0.81	0.82
−9	3.33	4.19	0.80	0.83
−6	3.33	4.17	0.80	0.85
−3	3.31	4.14	0.80	0.85
0	3.50	4.12	0.85	0.85

(b) Pacific Typhoon Belt (5°S to 30°N, 100°E to 180°)

Hour	Model rain (mm/day)	SSMI rain (mm/day)	Ratio (model/SSMI)	Correlation coefficient
−21	4.93	9.02	0.54	0.65
−18	6.97	9.03	0.77	0.80
−15	7.49	9.03	0.83	0.90
−12	7.28	9.03	0.81	0.92
−9	7.21	9.04	0.80	0.90
−6	7.46	9.04	0.83	0.91
−3	7.78	9.05	0.86	0.90
0	8.09	9.05	0.89	0.91

Overall, the model is able to retain rainfall rates of the order of 100 mm/day for all of the typhoons during the initialization.

We have carried out separate experiments to explore the relative roles of the reverse similarity, OLR matching and reverse cumulus parameterization during the preintegration phase. The largest impact was noted from the use of the reverse cumulus parameterization. Those results are separately reported in Mathur et al. (1992). The least impact comes from the OLR matching which did not appear to alter the forecasts of the wind field during the 5 days of integration. However, it had a marked positive impact on the prediction of the OLR. The surface fluxes appear to couple the ocean with the typhoons initially when the reverse similarity alone was invoked, but it does not improve the initialized rain or the forecasts as dramatically as the reverse cumulus parameterization.

6. Predicted fields

In this section, we present the results of two 5-day forecast experiments (the control and the SSM/I respectively). These forecasts were both carried out at the resolution T106.

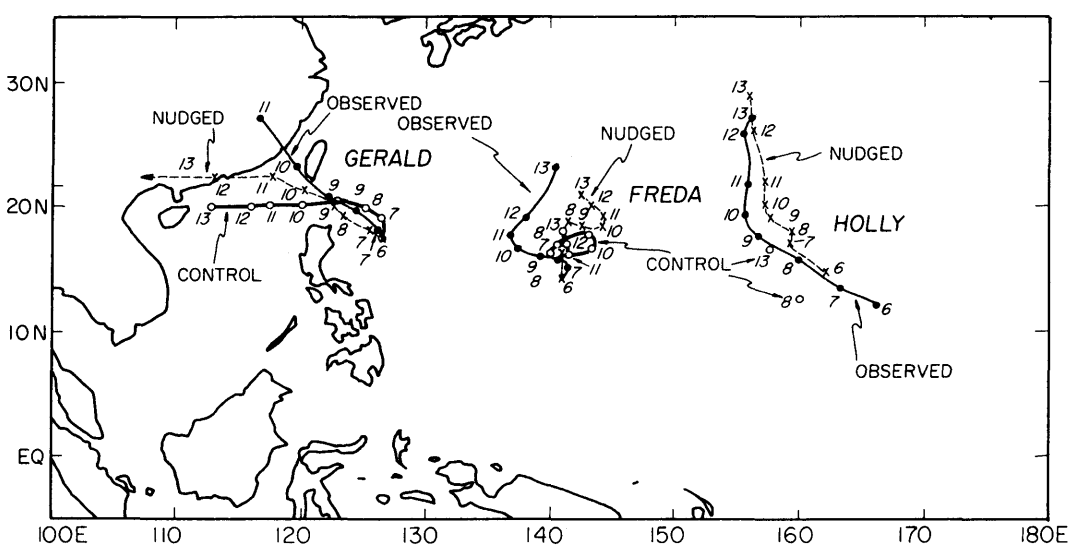

Fig. 8. Comparison of the observed and the predicted storm tracks for the control and the SSM/I experiments. The storm positions at intervals of 24 h are displayed.

6.1. Track of the typhoons

The observed and the predicted positions of the three typhoons are illustrated in Fig. 8. The best forecast for the SSM/I experiment was for the supertyphoon Holly. Freda was a slower moving storm over the central Pacific ocean. Its predicted track was somewhat erratic in the initial stages, however the position was considerably improved by 13 September, i.e., the 7 days of forecast with the SSM/I input. The forecast position of the westernmost storm (Gerald) for the first three days was quite close to the observed best track locations. Thereafter, the storm followed a more due westward track in the SSM/I based forecast. The control experiment exhibited a poor track for all three storms. The supertyphoon Holly did not develop at all; it appeared as a low pressure area on sea level on 8 and 13 September. Freda essentially formed a looping motion close to the initial position. The western most storm Gerald was handled reasonably well for the first three days by the control experiment, but thereafter the storm moved farther south of the SSM/I experiment. The central storm was difficult to handle by the control experiment since it was strongly influenced by the environmental flows, i.e., the descending motions in the surroundings of the other two storms.

6.2. Sea level pressure

The impact of the physical initialization on the sea level pressure forecasts is shown in Fig. 9 (a, b). The top panel shows the forecasts on day 4 for the control run, the bottom panel shows these results from the physical initialization run. The identity of the three typhoons are well retained in the physical initialization run; both experiments were able to retain the western most storm Gerald. The other two storms were not retained by the control run,

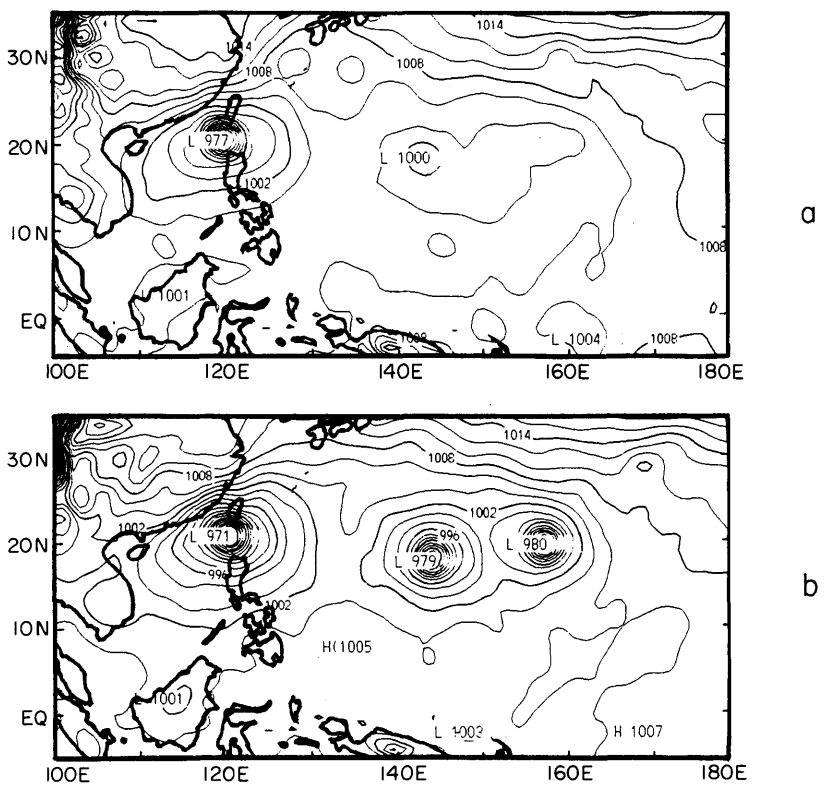

Fig. 9. Predicted fields of sea level pressure on day 4 of forecast. The top panel is for the control experiment and the bottom panel shows the results for the SSM/I experiment.

although a general weak low pressure area covers the region of these two storms. The SSM/I run was able to retain the sea level pressure of the storms through the 5 days.

6.3. *Prediction of rainfall*

A comparison of the predicted rainfall for the control experiment (top panel), the SSM/I initialized experiment (middle panel) and the observed rain based on SSM/I (bottom panel) are shown in Fig. 10 through Fig. 12. These illustrations respectively show the 24 hourly rainfall totals for days 0–1, 2–3, and 4–5 of the forecasts.

The model forecasts of the rain with the SSM/I input are much improved in comparison to the control experiment. The 24 hourly rainfall totals for the SSM/I experiment are somewhat larger than the observed measures. The three typhoons

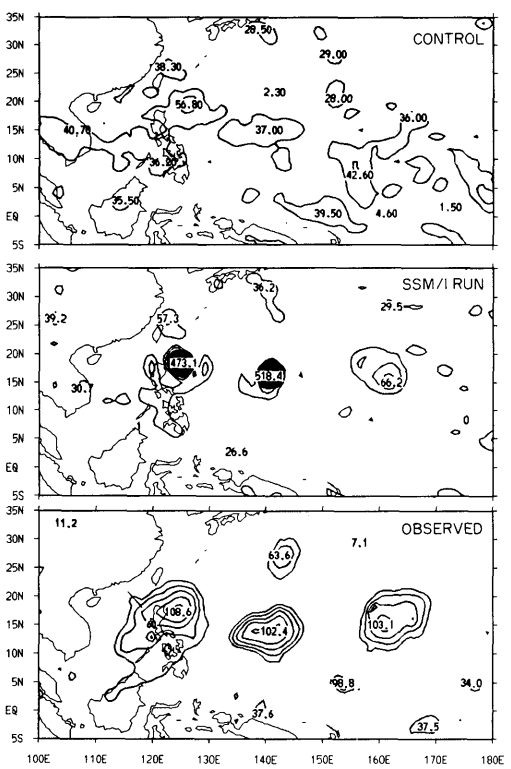

Fig. 10. Predicted and "observed" 24-h rainfall totals at the end of day 1. Units: mm/day. Interval: 20 mm/day. Top: Control experiment. Middle: SSM/I experiment. Bottom: "Observed".

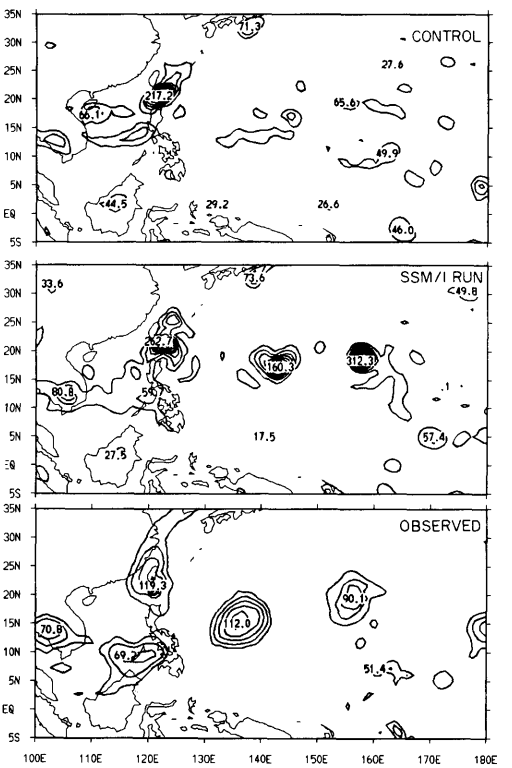

Fig. 11. Same as Fig. 10, but at the end of day 3 of forecast.

carry an observed maximum rainfall of around 108, 102 and 103 mm/day, respectively, for day 1 (see Fig. 10). The corresponding forecast values are 473, 518 and 66 mm/day. The model predictions are higher by almost a factor of two. These represent values at single transform grid points. However, an areal average around the storm has a very high accuracy. This may be seen from Table 3 presented in the concluding section. Figs. 11 and 12 show the observed and the predicted rain for days 3 and 5, again showing excessively large typhoon forecast rain as compared to the "observed" SSM/I measures. These are also again point values near the centers of the typhoons, which upon areal averaging show a much closer agreement. The resolution of the transform grid of the spectral model T106 near 20°N is around 95 km which is about one-third of the average resolution of the SSM/I data. The SSM/I initialization does seem to have a strong positive impact through the five days of forecasts.

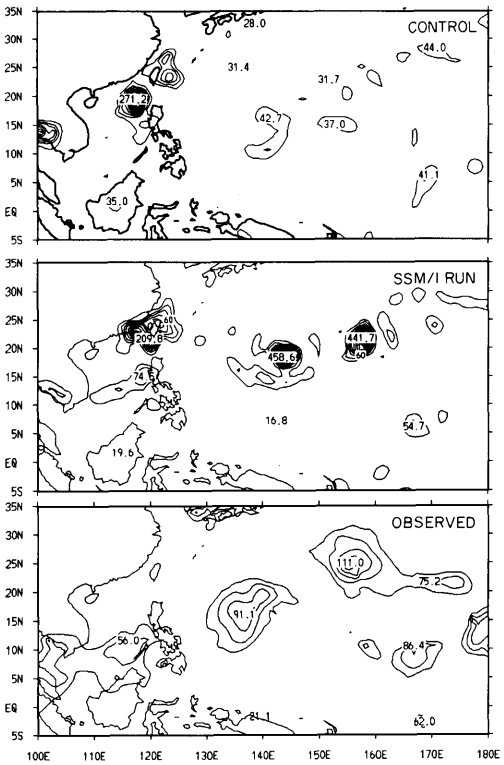

Fig. 12. Same as Fig. 10, but at the end of day 5 of forecast.

The spin-up of the rain by the model does appear to be very close to the SSM/I values over the Pacific ocean by hour 0, i.e., the initial state of the model. Given such an improvement in the initialization of prescribed rain the next obvious question is how well does the model retain the rainfall forecast skill. This is shown in Table 3 (a and b). Tables 3a and 3b show the forecast for the average rain over the global tropical belt and over the Pacific ocean. The respective vertical columns of this table are: rainfall predicted by the control run, that predicted with the SSM/I run, the observed rain based on SSM/I and OLR data sets, ratio of the control run to the observed rainfall, ratio of the SSM/I run to the observed rainfall and the correlation coefficients between control run and observed rainfall and between SSM/I run and observed rainfall. During the forecast from day 0 to day 5 the skill of the precipitation forecasts degrades considerably. However, we do see a higher forecast skill for the SSM/I experiment in comparison to the control. In summary the physical initialization handles the area averaged rain somewhat better than the control through the five days of forecast. The details of the typhoon rain, as seen in Figs. 10, 11 and 12, show that the SSM/I run is in fact vastly superior to the control run. This is perhaps a major result of the present study.

Table 3. *Comparison of rainfall forecast from control and nudged runs*

(a) Global tropical belt (30°S to 30°N)

Day	Rainfall control run (mm/day)	Rainfall nudged run (mm/day)	Rainfall SSM/I	Ratio (cont./SSMI)	Ratio (nudg./SSMI)	Correlation coefficient (cont., SSMI)	Correlation coefficient (nudg., SSMI)
1	5.60	5.67	4.20	1.33	1.35	0.28	0.62
2	6.55	5.82	3.74	1.75	1.56	0.32	0.36
3	5.22	5.38	3.73	1.40	1.44	0.25	0.22
4	4.54	4.85	4.81	0.94	1.01	0.15	0.15
5	4.11	4.35	4.32	0.95	1.01	0.12	0.12

(b) Pacific typhoon area (5°S–30°N, 100°E–180°E)

Day	Rainfall control run (mm/day)	Rainfall nudged run (mm/day)	Rainfall SSM/I	Ratio (cont./SSMI)	Ratio (nudg./SSMI)	Correlation coefficient (cont., SSMI)	Correlation coefficient (nudg., SSMI)
1	10.95	11.55	11.64	0.94	0.99	0.33	0.66
2	12.28	13.01	12.22	1.01	1.06	0.37	0.47
3	10.31	12.47	10.54	0.98	1.18	0.17	0.21
4	9.58	12.24	13.35	0.72	0.92	0.01	0.12
5	8.76	11.53	11.66	0.75	0.99	−0.04	0.04

However, it should be noted that the Olson algorithm has some defects and given another algorithm the model most likely could be made to relax to those values. Thus the model's spin-up of rain can be only as good as the rainrates we provide to it. Therefore, one must not interpret a correlation of 0.91 as indicative of a spin-up towards a prescribed "true observed rain". Hopefully the future rainfall measuring mission such as TRMM will provide us with further improvements on global tropical rainfall measurements.

6.4. Predicted motion field

A comparison of the observed and predicted motion field at 850 mb is presented in Figs. 13, 14 and 15. Here we have selected day 1, 3 and 5 of the forecasts for the observed, the control and the SSM/I experiments. Basically we see a better representation of the triple typhoon circulation for the SSM/I experiment through day 5 of forecasts. Although some semblance of a closed circulation is evident in the control experiment, it is the wind speed that degrades to rather low values. The collapse of the wind speed in the control forecasts are attributable to the lack of organization of the rainfall which is essential for the heating and maintenance of the warm core of the typhoons. The intensities of the storms in the control experiment were much underestimated for Holly and Freda. Gerald was located in a fairly data rich region and the performance of the control experiment was somewhat comparable to the SSM/I experiment through day 3 of the forecast.

The following results of the intensity forecasts are of interest.

(i) Typhoon Gerald, the western most storm: The observed maximum wind based on JTWC, Guam estimates at the end of day 1, 3 and 5 were 37, 45 and 15 ms^{-1}. The corresponding figures for the control experiments were 11, 34 and 39 ms^{-1}, while for the SSM/I experiment the respective estimates were 38, 39 and 48 ms^{-1}.

(ii) Typhoon Freda, the middle storm: The observed maximum wind based on JTWC, Guam estimates at the end of day 1, 3 and 5 were 35, 58 and 51 ms^{-1}. The control experiment had corresponding values of 5, 8 and 6 ms^{-1}, whereas for the SSM/I experiment the respective estimates were 24, 33 and 47 ms^{-1}.

(iii) Supertyphoon Holly, the eastern most storm. The observed maximum values of the wind speed based on JTWC, Guam were 51, 71 and 56 ms^{-1} at the end of days 1, 3 and 5. The corresponding values for the control forecast were 5, 5 and 7 ms^{-1} whereas for the SSM/I experiment the respective estimates were 12, 35 and 43 ms^{-1}. It is clear from the foregoing discussion that the physical initialization has had a positive impact on the intensity forecasts of the typhoons.

6.5. Improved water budget

With the introduction of the more realistic rain rates from the SSM/I in the detailed physical initialization phase we feel that the overall water budget in the model has been much improved. Here we shall examine the overall water budget over the storm region of the Pacific Ocean.

The relevant terms of the water budget are (i) change in precipitable water stored in the atmospheric column, (ii) surface evaporative flux, (iii) total precipitation (convective and nonconvective), and (iv) the lateral convergence of moisture flux.

The framework of the moisture equation in the FSU global spectral model is based on the dewpoint depression as a basic dependent variable. The budget equation is however cast in terms of the specific humidity q, i.e.,

$$\frac{\partial q}{\partial t} = -\nabla \cdot q\boldsymbol{V} - \frac{\partial}{\partial \sigma} q\dot{\sigma} + E - P, \tag{8}$$

where E denotes the evaporation and P the precipitation at any vertical σ level. The vertical integral of the above equation through the depth of the atmosphere provides the water budget equation for the total precipitation water $\bar{q}$, that can be averaged over a desired horizontal domain.

The equation,

$$\frac{\partial \bar{q}}{\partial t} = -\overline{\nabla \cdot q\boldsymbol{V}} + \bar{E} - \bar{P} \tag{9}$$

denotes the vertical integral. The terms on the left and right hand sides of equation (9) are calculated consistent with the computational scheme of the global model. As these terms are obtained exactly from the model, the water budget discussed here is residue free. A comparison of the water budget for the storm area of the three typhoons is illustrated

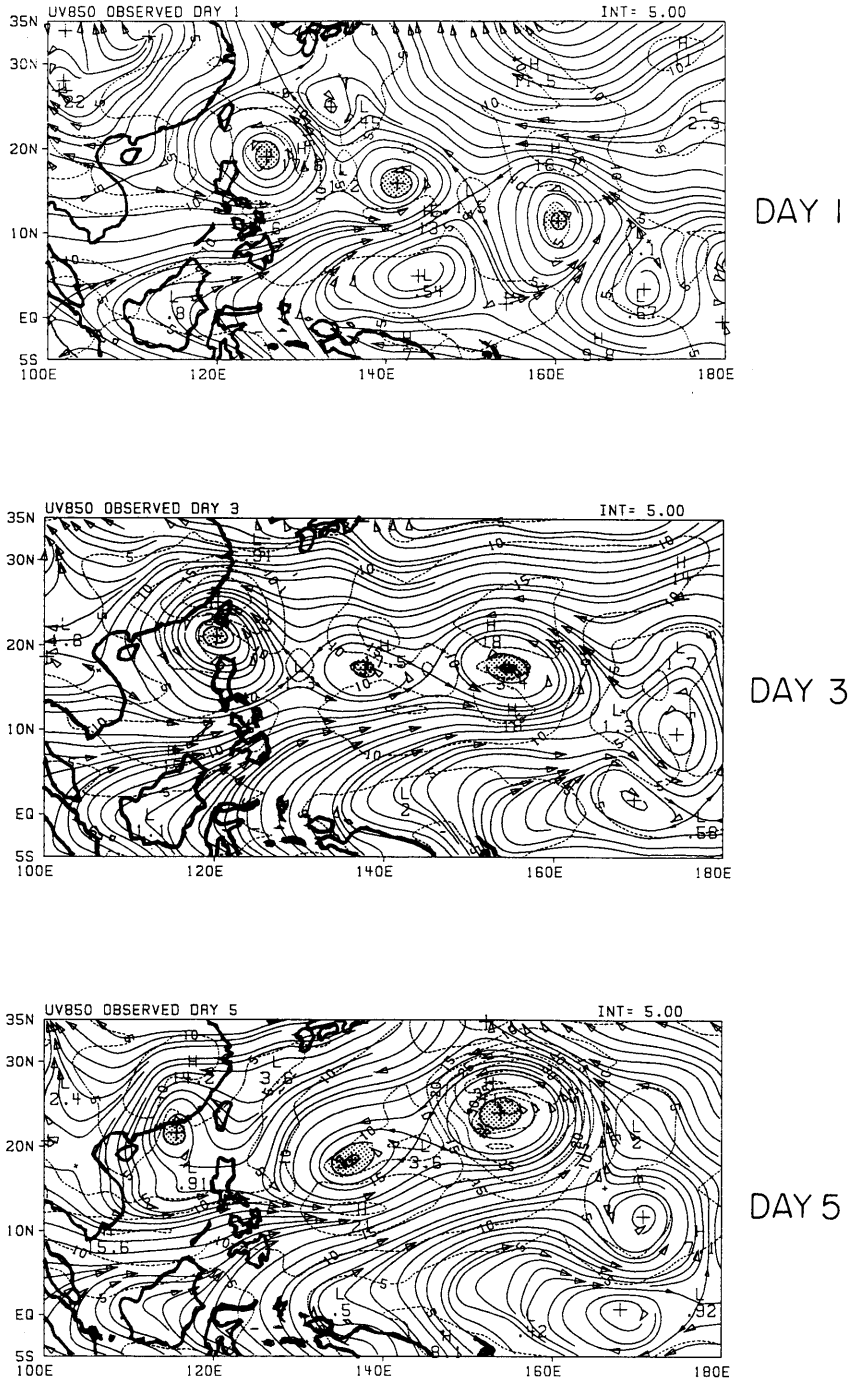

Fig. 13. 850 mb flows (streamlines and isotachs, ms^{-1}) for 7, 9 and 11 September 1987 at 1200 UTC based on ECMWF analysis.

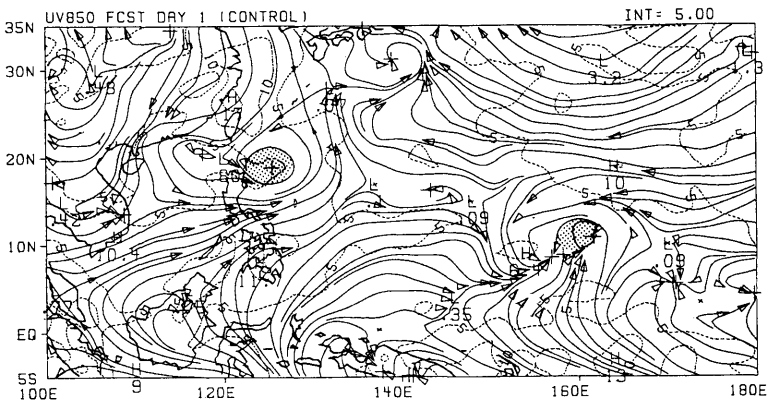

DAY 1

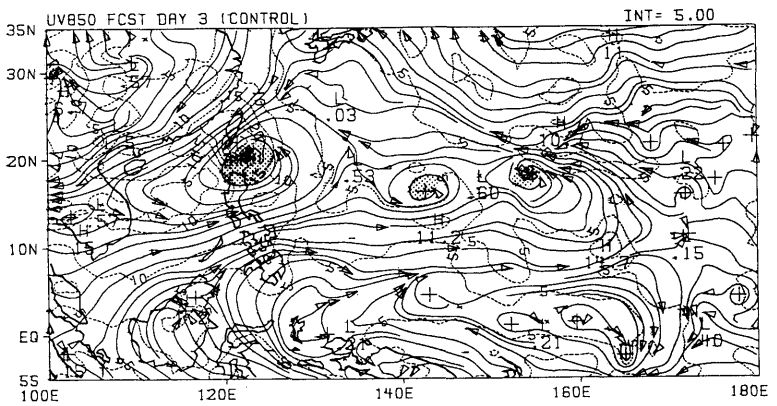

DAY 3

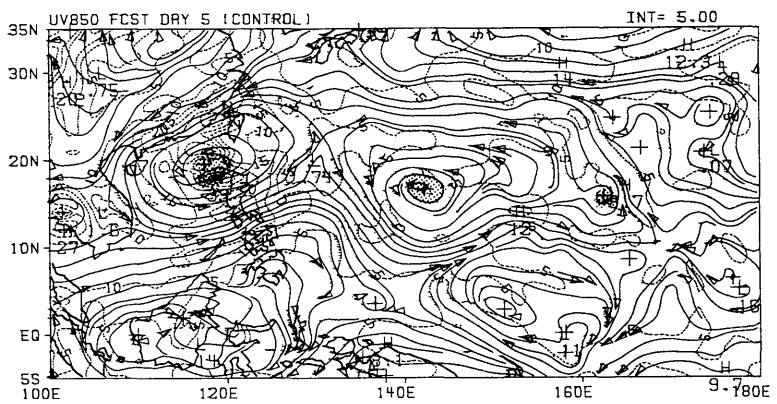

DAY 5

Fig. 14. 850 mb predicted flows (streamlines and isotachs ms^{-1}) for 7, 9 and 11 September 1987 at 1200 UTC based on the control experiment forecasts.

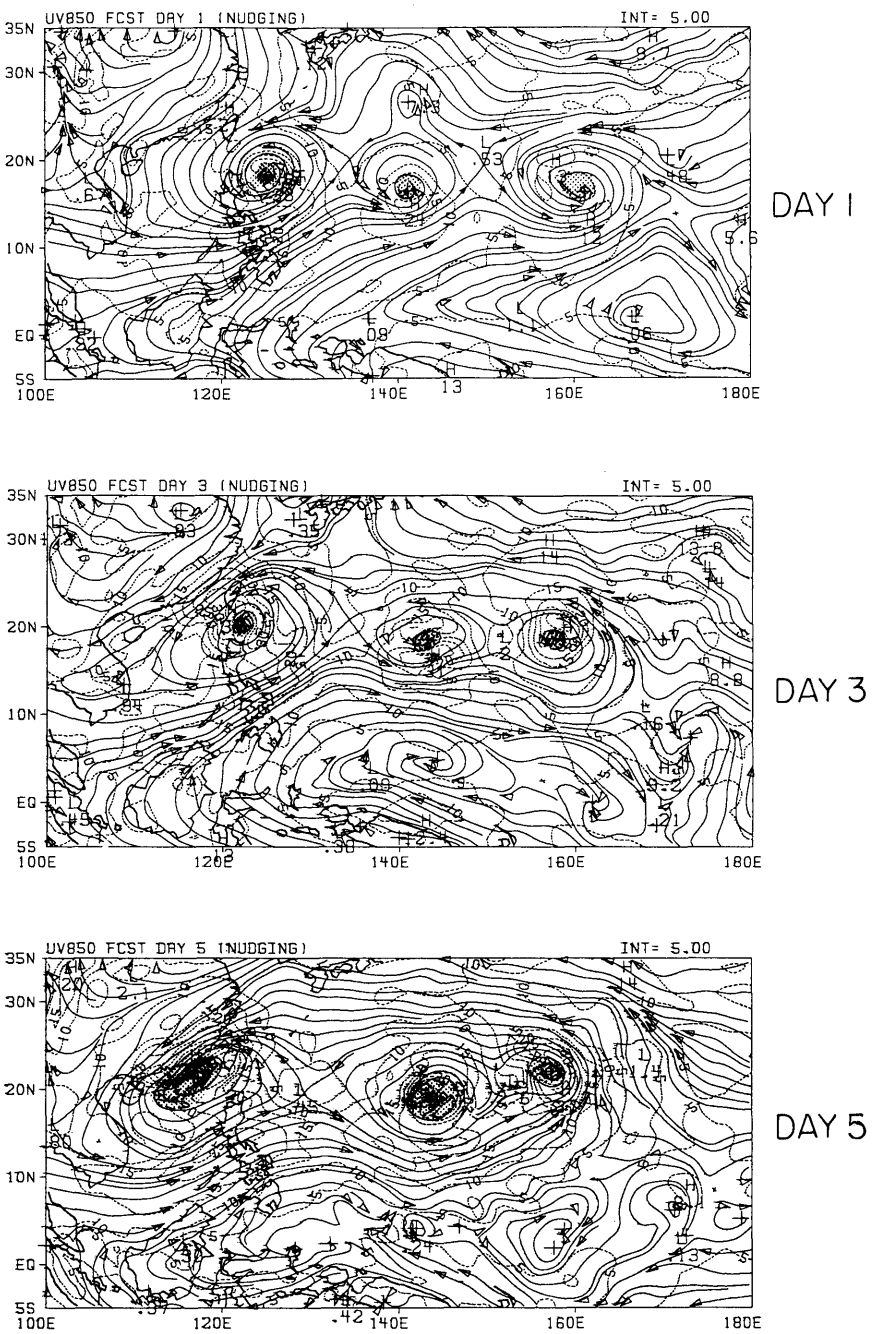

Fig. 15. Same as figure 16, but for the SSM/I experiment forecasts.

Table 4a. *Storm area (110–170°E, 10–25°N) total water budget (control) (unit: 10^9 metricton/day)*

Day	Local change	Evaporation	Rain	Convergence of flux
1	−29.8	64.1	153.8	59.9
2	−56.0	49.4	189.2	83.8
3	−53.0	50.4	167.9	64.5
4	−31.6	58.4	161.8	71.8
5	0.6	68.0	149.9	82.5
6	−6.6	64.7	142.6	71.3
7	−9.1	62.8	146.7	74.8

Table 4b. *Storm area (110–170°E, 10–25°N) total water budget (nudge) (unit: 10^9 metricton/day)*

Day	Local change	Evaporation	Rain	Convergence of flux
1	−23.9	65.6	213.4	123.9
2	−50.7	72.7	249.0	125.6
3	−44.1	76.9	210.3	89.3
4	−19.5	77.5	222.2	125.2
5	−9.6	83.5	230.2	137.1
6	−19.6	81.6	227.9	126.7
7	−23.7	67.8	177.1	85.6

in Tables 4a and 4b. This encloses a domain from 110°E to 170°E, 10°N to 25°N and through the troposphere. The columns respectively denote days, local change, evaporation, precipitation and the net horizontal convergence of flux. Basically what we see here is that the evaporation is somewhat smaller for the control experiment as compared to the SSM/I experiment; during days 2 and 3 of the forecasts the latter values were almost 20% higher. The latent heat fluxes at the surface level for the control and the SSM/I experiments are shown in Fig. 16. Here the left panel shows the fluxes for days 1, 3 and 5 of the forecast for the control and right panel shows those for the SSM/I experiment. In the SSM/I experiment, the fluxes increase to as much as 500 W/m^2 over the individual typhoons. An axis of strong latent heat flux develops along the Coast of China, as Typhoon Gerald approaches the coast. The strong fluxes are related to "strong along the shore northerly flows" near the east coast of China. Overall we note that all three typhoons show a strong coupling with the ocean even at day 5 for the SSM/I forecast. The control experiments, in contrast, showed a very weak organization of surface fluxes. The rainfall contributions to the water budget increase for the SSM/I by almost 22%; that increase in rainfall is largely accounted for by an increase in the convergence of flux of moisture for the SSM/I experiment. With the inclusion of the SSM/I rain rates in the physical initialization the typhoon circulations remain stronger and well maintained during the forecast; as a consequence the inflowing air is able to bring substantially more moisture into the storm's interior. Thus the horizontal convergence of flux is almost 50% larger for the SSM/I experiment as compared to the control.

This impact on the atmospheric water budget over the Pacific from the inclusion of SSM/I rain rate and the entire stream of the proposed physical initialization may be particularly relevant for the methodology to be developed for future programs such as GEWEX. We note markedly larger fluxes of latent heat across the ocean-atmosphere interface for the physical initialization experiment. The salient question of course remains as to what is the ground truth? Perhaps the improved numerical prediction of the motion field, i.e., the fact that the three typhoons were well maintained in the forecasts when the physical initialization was included, lends credence to the more robust fluxes at the initial time. The control experiment fails to maintain the typhoons so well, and weaker surface winds lead to somewhat weaker surface fluxes. The fluxes in the physical initialization experiment are internally consistent with larger rainfall rates, improved structure of the typhoons, stronger surface winds and a better description of the storm environment.

7. Concluding remarks

Current operational models have placed a major thrust on statistical optimal interpolation techniques towards improving the global analysis, Parish and Derber (1992). There is also considerable interest in the development of adjoints of

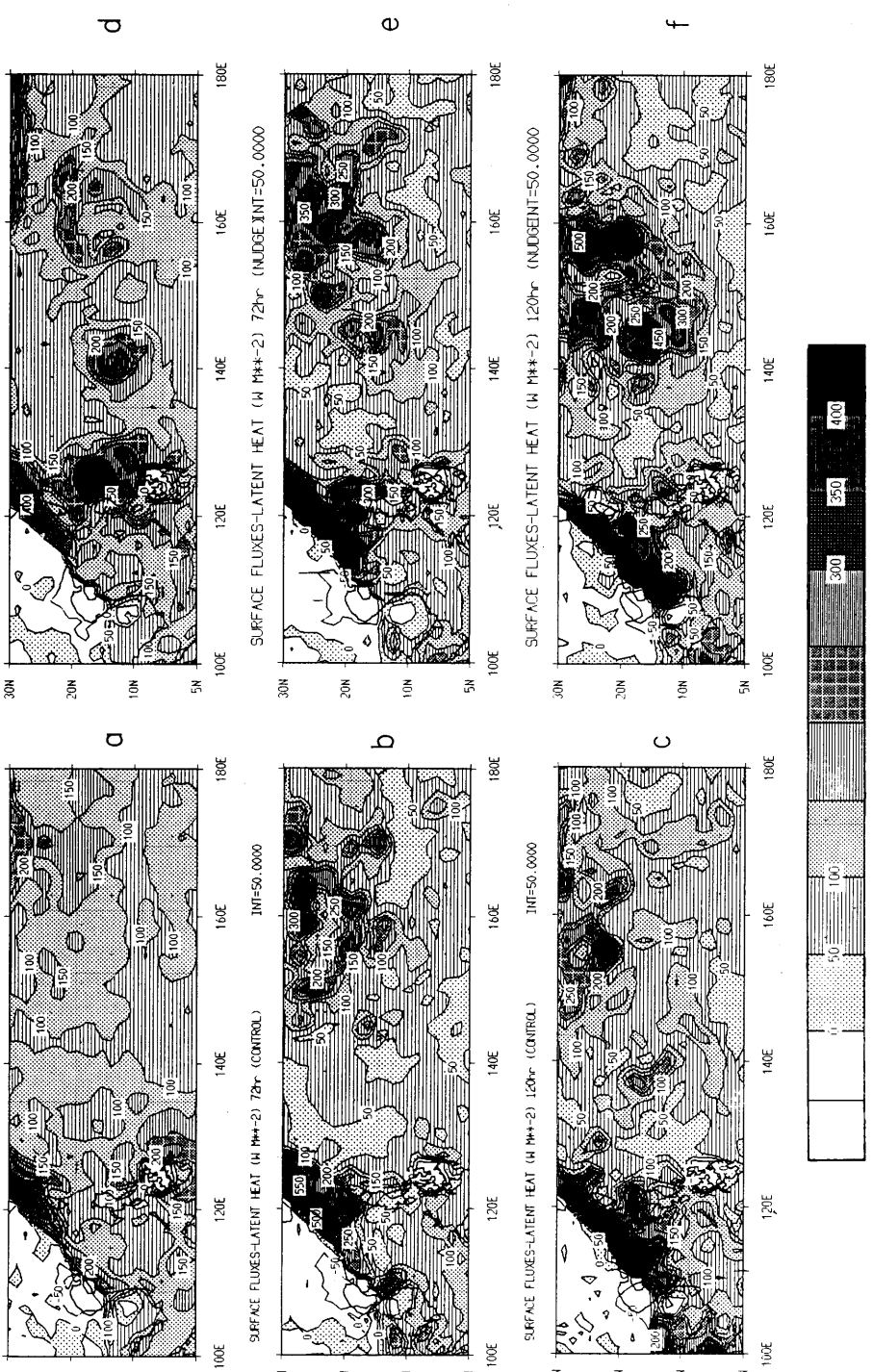

Fig. 16. Predicted surface fluxes of latent heat. The left panels a, b, c respectively show the results for forecasts at days 1, 3 and 5 for the control experiments. The right panels (d), (e) and (f) denote the same for the SSM/I experiment. Units: W/m^2.

global models for a consistent analysis of the data sets. Our experiments suggest that the incorporation of rain rates via the proposed reverse algorithms should be made a part of the analysis-assimilation cycle of an operational stream. The greatest benefits of these will be over the tropics; any major improvement of the tropical belt would have a beneficial impact on the medium range over the tropics. There are some difficulties in a straightforward application of the proposed method in an operational stream; we presuppose knowledge of a future streamfunction and surface pressure in our relaxation (nudging) process. Such would not be available to an operational assimilation. This may require a slight restructuring of the proposed method within an Optimal Interpolation (OI) or Statistical Interpolation (SI). Recent studies by Mathur et al. (1992) and Puri and Miller (1990) have explored the reverse cumulus parameterization and rainfall based heating in such a context, this is only one part of the proposed initialization. Further work is needed to address the entire stream of physical initialization within an analysis assimilation cycle.

The major contribution of this study appears in Tables 2 and 3. We show that the inclusion of SSM/I rain within the proposed physical initialization can be modelled to almost 80% to 90% via the reverse parameterization algorithms. That provides a correlation between the observed and the modelled rainfall of around 0.9 and is a major improvement over the results of the control experiment which does not include the observed rain within its initialization scheme. When this improved initialization is introduced in the prediction phase we note a gradual loss of accuracy of the predicted rain, however in comparison to the control we note a major improvement is clearly apparent. In principle the proposed physical initialization procedure can incorporate the rainfall from any reasonable rain rate algorithm. As further improvements in the measurements of rain rates arise, e.g., the forthcoming TRMM project, we expect a major impact of physical initialization on the medium range numerical weather prediction.

When a typhoon is already present at the initial time of a forecast, lacking observations to describe the initial typhoon (or hurricane), several propositions for the initial specification of a model vortex (i.e., bogussing) have been suggested by several authors, e.g., Andersson and Hollingsworth (1988), Mathur (1991), Thu and Krishnamurti (1992) and others. The typhoon motion appears to be related to the azimuthal asymmetries of the storm's circulation (Holland, 1984). Lack of data generally prevents an analysis to provide an adequate definition of such asymmetries. Bogussing procedures usually entail parameters such as storm intensity, size and past motion (Mathur, 1991; Thu and Krishnamurti, 1992). Such parameters alone do not guarantee the recovery of proper asymmetries.

The other possible alternative might be to spin-up these data deficient vortices via the proposed physical initialization. The spin-up of rain and associated diabatic heating in a physical initialization within a nudging phase generates some detailed asymmetries of the storm's structure. The storm size, intensity and past motion are essentially contained within the satellite's definition of rain. The addition of the diabatic process adds further information i.e., beyond what the purely bogussing exercise provides. The success of such an alternative was demonstrated by Puri and Miller (1990) in a recent study. In this study the satellite derived OLR rain was used to define the diabatic heating within a 4D-assimilation scheme. The tropical cyclones north of Australia were handled reasonably well by this assimilation. In contrast, the control experiments lacking satellite OLR rain were quite deficient in describing the initial strength of the tropical cyclones. Yap (1992) used a similar physical initialization procedure in the context of a tropical mesoscale model. The forecast runs after physical initialization improved the prediction of a tropical depression and rainfall greatly as compared to control runs. Physical initialization within a nudging phase or within a 4D assimilation appears to be a viable alternative. We feel that the addition of meso-scale rainfall details from products such as the SSM/I can add a lot to the physical initialization and to the definition of the initial state of a typhoon.

A number of major initiatives, e.g., TOGA, Coupled Ocean Atmospheric Response Experiment (TOGA-COARE), Tropical Rainfall Measuring Experiment (TRMM) and Global Energy and Water Cycle Experiment (GEWEX) address the need for improvements of surface fluxes. Preparation of global rain rates, subjected to consistent physical initialization, can provide very useful data sets for these programs.

8. Acknowledgements

This work was jointly supported by Navy grant no: N00014-89-J-1476, NSF grant no: ATM 8812053 and NASA grant no: NAG 5-1595. The computation described here were carried out on the CRAY/YMP at NCAR which is sponsored by the National Science Foundation and on the CRAY/YMP at the Supercomputer Computational Research Institute (SCRI) of Florida State University.

REFERENCES

Andersson, E. and Hollingsworth, A. 1988. *A typhoon bogus observations in the ECMWF data assimilation system.* Tech. Memo. No. 148, ECMWF, 25 pp. Available from the European Center for Medium range weather forecast. Shinfield Park, Berkshire, England.

Businger, J. A., Wyngard, J. C., Izumi, Y. and Bradley, E. F. 1971. Flux profile relationship in the atmosphere surface layer. *J. Atmos. Sci. 28*, 181–189.

Gairola, R. K. and Krishnamurti, T. N. 1992. Rain rates based on SSM/I, OLR and raingauge data sets. *J. Meteorol. Atmos. Phys. 50*, 165–174.

Harshvardan and Corsetti, T. G. 1984. *Long-wave parameterization for the UCLA/GLAS GCM.* NASA Tech. Memo. 86072, Goddard Space Flight Center, Greenbelt, MD 20771, 52 pp.

Holland, G. J. 1984. Tropical cyclone motion: A comparison of theory and observations. *J. Atmos. Sci. 41*, 68–75.

Janowiak, J. E. and Arkin, P. A. 1991. Rainfall variations in the tropics during 1986–89, as estimated from observations of cloud top temperatures. *J. Geophys. Res. 96*, suppl., 3359–3373.

Joint typhoon Warning Center, Guam, 1987. 1987 *Annual tropical cyclone report*, 213 pp.

Kanamitsu, M., Tada, K., Kudo, K., Sato, N. and Isa, S. 1983. Description of the JMA operational spectral model. *J. Met. Soc. Japan 61*, 812–828.

Kanamitsu, M. 1975. *On numerical prediction over a global tropical belt.* Report no. 75–1, Dept. of Meteorology, Florida State University, Tallahassee, Florida 32306, pp. 1–282.

Kitade, T. 1983. Nonlinear normal mode initialization with physics. *Mon. Wea. Rev. 111*, 2194–2213.

Krishnamurti, T. N., Xue, J., Bedi, H. S., Ingles, K. and Oosterhof, D. 1991. Physical initialization for numerical weather prediction over the tropics. *Tellus 43AB*, 53–81.

Krishnamurti, T. N., Low-Nam, S. and Pasch, R. 1983. Cumulus parameterization and rainfall rates II. *Mon. Wea. Rev. 111*, 816–828.

Kuo, H. L. 1965. On formation and intensification of tropical cyclones through latent heat release by cumulus convection. *J. Atmos. Sci. 22*, 40–63.

Kuo, H. L. 1974. Further studies of the parameterization of the influence of cumulus convection on large scale flow. *J. Atmos. Sci. 31*, 1232–1240.

Lacis, A. A. and Hansen, J. E. 1974. A parameterization of the absorption of solar radiation in the earth's atmosphere. *J. Atmos. Sci. 31*, 118–133.

Louis, J. F. 1979. A parametric model of vertical eddy fluxes in the atmosphere. *Boundary Layer Meteorology 17*, 187–202.

Mathur, M. B. 1991. The National Meteorological Center's Quasi-Lagrangian Model for hurricane prediction. *Mon. Wea. Rev. 119*, 1419–1447.

Mathur, M. B., Bedi, H. S., Krishnamurti, T. N., Kanamitsu, M. and Woollen, J. S. 1992. Use of satellite derived rainfall for improving tropical forecasts. *Mon. Wea. Rev. 120*, 2540–2560.

Olson, W. S., Fontaine, F. S., Smith, W. L. and Achtor, R. H. 1990. *Recommended algorithms for the retrieval of rainfall rates in the tropics using SSM/I (DMSP-F8).* Manuscript, University of Wisconsin, Madison, 10 pp.

Parish, D. F. and Derber, J. C. 1992. The National Meteorological Center's Spectral Statistical, Interpolation analysis system. *Mon. Wea. Rev. 120*, 1747–1763.

Puri, K. and Miller, M. J. 1990. The use of satellite data in the specification of convective heating for diabatic initialization and moisture adjustment in numerical weather prediction models. *Mon. Wea. Rev. 118*, 67–93.

Tiedtke, M. 1984. The sensitivity of the time-mean large-scale flow to cumulus convection in the ECMWF model. *Worshop on Convection in large-scale numerical models.* ECMWF, 28 Nov.–1 Dec. 1983, 297–316.

Thu, T. V. and Krishnamurti, T. N. 1992. Vortex initialization for typhoon track prediction. *J. Meteorol. Atmos. Phys. 47*, 1–10.

Wallace, J. M., Tibaldi, S. and Simmons, A. J. 1983. Reduction of systematic forecast errors in the ECMWF model through the introduction of envelope orography. *Quart. J. Roy. Met. Soc. 109*, 683–718.

Yanai, M., Esbensen, S. and Chu, J. H. 1973. Determination of bulk properties of tropical cloud clusters from large-scale heat and moisture budgets. *J. Atmos. Sci. 30*, 611–627.

Yap, K. S. 1992. *Impact of Newtonian assimilation and physical initialization on the initialization and prediction of a tropical mesoscale model.* Report no. 92–2. Department of Meteorology, Florida State University, Tallahassee, FL 32306, 230 pp.